HHS Public Access

Author manuscript

J Extracell Biol. Author manuscript; available in PMC 2024 February 28.

Published in final edited form as:

J Extracell Biol. 2022 July ; 1(7): . doi:10.1002/jex2.50.

Protein palmitoylation regulates extracellular vesicle production and function in sepsis

Xiaoyuan Yang[1], **Ethan Zheng**[1], **Victor Chatterjee**[1], **Yonggang Ma**[1], **Amanda Reynolds**[1], **Nuria Villalba**[1], **Mack H. Wu**[1], **Sarah Y. Yuan**[1,2]

[1]Department of Molecular Pharmacology and Physiology, University of South Florida Morsani College of Medicine, Tampa, Florida, USA

[2]Department of Surgery, University of South Florida Morsani College of Medicine, Tampa, Florida, USA

Abstract

Extracellular vesicles (EVs) are bioactive membrane-encapsulated particles generated by a series of events involving membrane budding, fission and fusion. Palmitoylation, mediated by DHHC palmitoyl acyltransferases, is a lipidation reaction that increases protein lipophilicity and membrane localization. Here, we report palmitoylation as a novel regulator of EV formation and function during sepsis. Our results showed significantly decreased circulating EVs in mice with DHHC21 functional deficiency (*Zdhhc21*$^{dep/dep}$), compared to wild-type (WT) mice 24 h after septic injury. Furthermore, WT and *Zdhhc21*$^{dep/dep}$ EVs displayed distinct palmitoyl-proteomic profiles. Ingenuity pathway analysis indicated that sepsis altered several inflammation related pathways expressed in EVs, among which the most significantly activated was the complement pathway; however, this sepsis-induced complement enrichment in EVs was greatly blunted in *Zdhhc21*$^{dep/dep}$ EVs. Functionally, EVs isolated from WT mice with sepsis promoted neutrophil adhesion, transmigration, and neutrophil extracellular trap production; these effects were significantly attenuated by DHHC21 loss-of-function. Furthermore, *Zdhhc21*$^{dep/dep}$ mice displayed reduced neutrophil infiltration in lungs and improved survival after CLP challenges. These findings indicate that blocking palmitoylation via DHHC21 functional deficiency can reduce sepsis-stimulated production of complement-enriched EVs and attenuates their effects on neutrophil activity.

Correspondence: Sarah Y. Yuan, Departments of Molecular Pharmacology & Physiology and Surgery, University of South Florida Morsani College of Medicine, 12901 Bruce B. Downs Blvd., MDC 8, Tampa, FL 33612, USA. syuan@usf.edu.

AUTHOR CONTRIBUTIONS

Xiaoyuan Yang performed, analyzed, interpreted the experiments, and drafted the manuscript. Ethan Zheng, Victor Chatterjee, and Amanda Reynolds assisted with most of the experiments. Yonggang Ma assisted with neutrophil assays and data interpretation. Mack H. Wu assisted with palmitoylation assay and data interpretation. Yonggang Ma, Nuria Villalba, Ethan Zheng, and Sarah Y. Yuan edited and revised the manuscript. Sarah Y. Yuan initiated, directed, and sponsored the work throughout all levels of development. All authors approved it for publication.

CONFLICT OF INTEREST

None.

SUPPORTING INFORMATION

Additional supporting information can be found online in the Supporting Information section at the end of this article.

Keywords

complement pathways; extracellular vesicles; neutrophil activation; protein palmitoylation; septic injury

1 | INTRODUCTION

Circulating extracellular vesicles (EVs) are membrane-enclosed, nano-sized particles secreted by various types of cells (Chatterjee, Yang, Ma, Wu et al., 2020; Wen et al., 2017). These vesicles effectively mediate intercellular communication by transferring cargos containing proteins, nucleic acids, and lipids (Cocozza et al., 2020; Kalluri & Lebleu, 2020; Théry et al., 2018). Viable cells mainly produce EVs through membrane budding, fission and fusion (Teng & Fussenegger, 2020). More specifically, small EVs (<100 nm) are primarily originated from inward budding of endosomal membranes to form multivesicular bodies (MVBs) containing intraluminal vesicles (ILVs) (Kalluri & Lebleu, 2020), a process requiring two membrane-associated protein families: tetraspanins and endosomal sorting complex required for transport (ESCRT) complex (Abels & Breakefield, 2016; Andreu & Yáñez-Mó, 2014; Pegtel & Gould, 2019). Once mature, small EVs are released into extracellular space via fusion of MVBs with plasma membrane under the regulation of small GTPases and other membrane proteins (Hessvik & Llorente, 2018). In contrast, large EVs (100–1000 nm) are mainly generated by outward budding of plasma membrane as a result of phospholipid redistribution and cytoskeletal protein contraction (Théry et al., 2018). Emerging evidence has demonstrated an association between circulating EV numbers and various diseases (Hoshino et al., 2020; Manier et al., 2017). However, the molecular mechanisms regulating EV production under pathological conditions are not fully elucidated.

The biological and pathological functions of EVs are determined by their cargo content. A great number of bioactive molecules are highly enriched in EVs, and EV cargo content selection is mediated by tetraspanins and ESCRTs during EV formation (Andreu & Yáñez-Mó, 2014; Vietri et al., 2020). Once released into the circulation, EV cargo molecules are more stable for extended periods, compared to other circulating factors, and they are less likely to be targeted for enzymatic destruction due to the protection of lipid bilayer (Boukouris & Mathivanan, 2015; Rontogianni et al., 2019). EVs are efficient mediators of cell-cell communication because the lipophilic nature of EVs allows them to easily dock on cell surface and fuse with cell membrane, thereby rapidly delivering their content to recipient cells. Thus, EVs are capable of directly altering signalling cascades and cellular events of recipient cells, bypassing the need to activate membrane receptors (Rontogianni et al., 2019). Several lines of evidence show that EVs play essential roles in many pathological processes and contribute to the progression of various diseases (Clement et al., 2020; Crewe et al., 2018; De Abreu et al., 2020; Xu et al., 2018). For instance, EVs have been reported to participate in innate immune responses, infectious diseases, and immunological disorders through delivering inflammatory cargos such as cytokines and complement components (Biro et al., 2007; Karasu et al., 2018; Robbins et al., 2016; X. Zhou et al., 2020). Our previous study has also shown that EVs produced under inflammatory stimulation promote

neutrophil adhesion, transmigration, and neutrophil extracellular trap (NET) formation (Chatterjee, Yang, Ma, Cha, et al., 2020). Therefore, it is of great importance to understand the regulatory mechanisms of EV production and molecular composition.

Palmitoylation is the covalent attachment of a 16-carbon palmitic acid on cysteine residues of a protein, a reversible post-translational modification catalyzed by palmitoyl acyltransferases (PATs) containing aspartate-histidine-histidine-cysteine (DHHC) motif (Beard et al., 2016). Palmitoylation is crucial for the proper function of membrane and membrane-associated proteins. The attached lipophilic palmitic acid maintains protein conformation, prevents degradation, and facilitates protein interaction with other proteins containing lipophilic groups (Yang et al., 2020). Many membrane proteins involved in EV biogenesis such as tetraspanins, ESCRT components, and small GTPases are palmitoylation substrates (Bastin & Heximer, 2013; Modica et al., 2017; Navarro-Lérida et al., 2012; Romancino et al., 2018; Sharma et al., 2008). Through regulating these proteins, palmitoylation is highly likely to affect various aspects of EV production, including ILV formation, EV release, and plasma membrane budding. Furthermore, the attached long fatty acid chains drastically increase the lipophilicity of a protein, promoting its transfer and stable anchoring onto cellular membranes (Yang et al., 2020). Previous studies have shown that palmitoylation targets modified cytoplasmic proteins to the sites of membrane budding, leading to their presence in secreted vesicles (Fang et al., 2007; Shen et al., 2011). Consistently, three-fold enrichment of palmitoylated proteins is found in EV proteome compared to human proteome (Mariscal et al., 2020). The distribution of palmitoylated proteins shows that EVs contain the highest percentage of palmitoylated proteins compared to other subcellular compartments (Romancino et al., 2018). Moreover, the loading of several cargo proteins onto EVs has been shown to be affected by palmitoylation (Carnino et al., 2020; Mariscal et al., 2020; Romancino et al., 2018; Verweij et al., 2015). Collectively, these findings suggest that protein palmitoylation and DHHCs may be important regulators of EV production and cargo sorting.

Currently, there is limited information available regarding the palmitoyl-protein contents of circulating EVs in physiological or pathological conditions, and the role of palmitoylation in regulating EV biogenesis under these conditions remains poorly understood. In recent studies, we identified a significantly increased plasma level of EVs in patients and animals with trauma and sepsis, correlating with exacerbated proinflammatory response and cellular injury (Beard et al., 2016). We also observed greatly increased palmitoylation and DHHC21 activity under inflammatory conditions (Beard et al., 2016; Yang et al., 2021). DHHC21, unlike other DHHCs, is localized in plasma membrane, which allows it to dynamically regulate the function of many plasma membrane-associated proteins involved in EV generation, such as G protein-coupled receptors, G proteins, and phospholipases (Beard et al., 2016; Fan et al., 2020; Yang et al., 2021). In the present study, we sought to determine if DHHC21-mediated palmitoylation affects EV production, cargo content, and function during sepsis. Comparing wildtype (WT) mice and DHHC21 functionally deficient *Zdhhc21*$^{dep/dep}$ mice, we found that palmitoylation contributed to sepsis-stimulated EV production. A comprehensive analysis of EV palmitoyl proteomes revealed decreased complement components in *Zdhhc21*$^{dep/dep}$ EVs compared to WT EVs after sepsis. Functionally, EVs from *Zdhhc21*$^{dep/dep}$ mice were less capable of promoting neutrophil

activation compared to EVs from WT mice after septic injury. Moreover, *Zdhhc21*$^{dep/dep}$ mice exhibited reduced neutrophil recruitment to lungs and decreased mortality after CLP. These data suggest palmitoylation as a novel regulator of EV formation and function under septic conditions.

2 | MATERIALS AND METHODS

2.1 | Reagents

All reagents are listed in Supplementary Table S1.

2.2 | Animals

Zdhhc21$^{dep/dep}$ mice and their wild-type control mice (B6C3Fe) were purchased from Jackson Laboratory. The genotype and phenotype of *Zdhhc21*$^{dep/dep}$ mice were reported in our previous publications (Beard et al., 2016; Yang et al., 2021). Mice were housed under a 12/12 h light/dark cycle with food and water available ad libitum. Both male and female mice (16–20 weeks) were used for this study. All animal surgical procedures are approved by the University of South Florida Institutional Animal care and Use Committee and conform to the NIH Guide for the Care and Use of Laboratory Animals. This study was carried out in compliance with the ARRIVE guideline.

2.3 | Cecal ligation and puncture

Mice were anaesthetized with isoflurane (3% induction and 1% maintenance) and placed on a heating pad. Sustained-release Buprenorphine (1 mg/kg) was injected subcutaneously for analgesia. After shaving and disinfection, 1 cm of midline incision was made in the abdominal area to expose the cecum. The exteriorized cecum was tightly ligated at 5 mm below the ileocecal valve using a sterile suture. A 20-gauge needle was used to perforate the cecum twice distal to the ligation site (Yang et al., 2018). 37°C Lactated Ringer solution was treated topically to prevent the cecum from drying. After closing the abdominal region, the mice were given 1 ml of 37°C saline subcutaneously for fluid resuscitation. Mice in sham group were subjected to the same procedures except the ligation and puncture. For survival study, mice were monitored for 72 h after CLP.

2.4 | EV isolation and quantification

Mouse blood was collected via cardiac puncture 24 h after sham surgery or CLP. Platelet poor plasma (PPP) was generated by sequentially centrifuging the blood at 250 g for 30 min at room temperature, 2500 g for 30 min, and 12,000 g for 5 min at 4°C. (Chatterjee, Yang, Ma, Cha, et al., 2020) Crude EV was prepared by ultracentrifugation of PPP at 100,000 g for 2 h at 4°C. EV pellet was then resuspended and purified using size-exclusion chromatography qEV10 column per manufacture's instruction (Böing et al., 2014; Konoshenko et al., 2018). Eluted fractions were tested for the number of EVs and protein concentration via nano-tracking analysis and Bradford protein assay, respectively. EV-enriched and plasma protein poor fractions (fractions 5–9) were pooled to collect purified EVs. The number and size of EVs were measured by Nanosight NS300 system (Malvern Instruments Ltd). EV samples were diluted 1:50 and pumped into the system through 1 ml syringe. Each measurement was recorded in a set of five videos (60 s each)

with the camera level at 9. The recordings were then analyzed using detection threshold of 2 and screen gain of 9 (Vestad et al., 2017).

2.5 | Transmission electron microscopy

EVs were isolated and purified as mentioned above. EVs were fixed with 2% paraformaldehyde in 0.1M sodium cacodylate for 10 min. After washing two times with 0.1 M sodium cacodylate, 5 μl of EV suspension was loaded onto formvar coated 200 mesh copper EM grids. 1% uranyl acetate (UA) was added to the grid to stain EVs for 30 s. Excessive UA was removed by contacting the grid edge with filter paper (Jung & Mun, 2018). The grid with stained EVs was then washed and dried at room temperature. Images were captured using transmission electron microscope (JEOL1400, Tokyo, Japan).

2.6 | Resin-assisted capture

Palmitoylated proteins on EVs were isolated using resin-assisted capture as previously described (Beard et al., 2016; Mariscal et al., 2020; Yang et al., 2021). EV samples were lysed in lysis buffer (100 mM HEPES, 25 mM NaCl, 1 mM EDTA, 10 μM palmostatin B, Roche protease inhibitor tablet, pH 7.4). The lysate was then blocked with blocking buffer (100 mM HEPES, 1 mM EDTA, 2.5% SDS, 6 μl/ml MMTS, pH 7.4) at 50°C for 30 min with constant vortexing. Four volume of cold acetone (100%) was added to allow the proteins to precipitate overnight at −20°C. After centrifugation at 5000 g for 30 min, protein pellet was washed five times with 70% acetone and resuspended into binding buffer (100 mM HEPES, 1 mM EDTA, 1.0% SDS, pH 7.4). Following the normalization of protein concentration among groups, each protein sample received the same amount of Thiopropyl Sepharose 6B beads and 0.2 M of hydroxylamine. After 4 h of incubation on a rotator, palmitoylated proteins were eluted using 50 mM DTT in 1× sample buffer.

2.7 | Liquid chromatography-tandem mass spectrometry (LC-MS/MS) analysis and data processing

Palmitoylated proteins were loaded onto a 4%–20% Tris-Glycine gel. Electrophoresis was stopped immediately after all the proteins run into the gel. The gel was washed, stained with Coomassie Blue Stain, and sent to Weill Cornell Medicine Proteomics and Metabolomics Core Facility for LC-MS/MS analysis. The data were processed by MaxQuant and searched against Uniprot mouse protein database. Protein intensities were normalized to correct the sample loading differences. Student's *t*-test was applied to calculate *p*-value; multiple hypothesis correction was performed using Benjamini Hochberg method to obtain adjusted *p*-value. Protein expression pattern of different groups was compared using heatmap hierarchical clustering analysis.

2.8 | Palmitoyl-proteome analysis

Palmitoyl-proteome identified by LC-MS/MS was compared with Mus musculus SwissPalm database (https://swisspalm.org/) to determine the percentage of high-confidence palmitoylated proteins (B. Zhou et al., 2019). Mapping previously reported EV proteins was conducted by cross-checking the palmitoyl-proteome with Mus musculus Vesiclepedia (http://microvesicles.org/) and ExoCarta database (http://www.exocarta.org/) (Rontogianni

et al., 2019). Protein classification was performed using Gene Ontology Panther Classification System (http://www.pantherdb.org/). Gene ontology enrichment analysis was conducted on Database for Annotation, Visualization and Integrated Discovery (DAVID) 6.8 platform (https://david.ncifcrf.gov/home.jsp) using the gene name of all the identified proteins. Disease enrichment analysis was performed using ToppCluster (https://toppcluster.cchmc.org/) and visualized using Cytoscape 3.8.2. Principle component analysis was conducted via ClustVis (https://biit.cs.ut.ee/clustvis/).

Ingenuity pathway analysis-—palmitoyl-protein IDs, log2 value, *p*-value, and adjusted *p*-value were uploaded to QIAGEN Ingenuity Pathway Analysis Software V 01–19-02. Analysis cut off was set as $p < 0.05$. *z*-Score was calculated by IPA software to infer the activation (positive *z*-score) or the inhibition (negative z-score) state of a given pathway/function. Most significantly affected pathways were determined by *z*-score based canonical pathway analysis. Diseases and Function analysis was performed to categorize differently expressed proteins into specific diseases or functions. *p*-Value of a given disease function was calculated by IPA software using Fisher Exact Tests. (Krämer et al., 2014; Yu et al., 2016) The effects of differently expressed proteins on complement activation pathway were predicted based on z-score.

2.9 | Western blotting

Fractions 5–9 were lysed with 1× RIPA buffer containing protease inhibitors. The lysates were loaded onto 4%–20% Tris-Glycine gel. After electrophoresis, proteins were transferred onto nitrocellulose membrane using Trans-Blot Turbo. The membrane was then blocked for 1 h and incubated with rabbit anti-CD9 primary antibody (1:1000) or rabbit anti-CD81 primary antibody (1:1000) overnight at 4°C. Following three times of washing with PBST, the membranes were then probed with IRDye800CW donkey anti-rabbit secondary antibody (1:20,000) for 45 min at RT. Mouse IgG was detected using IRDye800CW donkey anti-mouse IgG antibody (1:20,000). Membranes were then washed three times with PBST and imaged using Li-COR Odyssey.

2.10 | Cell culture

Mouse lung pulmonary endothelial cells were cultured in Mouse Endothelial Cell Medium with supplement kit at 37°C ina 5% CO2 humidified incubator. Cells were seeded on 0.1% gelatin pre-coated coverslips or transwell plates and grown into confluence (Yang et al., 2018).

2.11 | Neutrophil function analysis

Neutrophil isolation-—mouse blood was collected through cardia puncture using a heparinized syringe. Red blood cells were lysed using Ammonium-Chloride-Potassium Lysing Buffer. Neutrophils were then isolated using anti-Ly-6G microbeads per manufacturer's instruction. The number and viability of the isolated neutrophils were determined by LUNA II Automated Cell Counter.

Neutrophil adhesion-—MLMVECs were pre-stimulated with 100 ng/ml TNF-α for 4 h and rinsed three times with warm HBSS. EVs from different groups were normalized

to the same concentration. 1×10^5 neutrophils were incubated with 100 μl EVs (~10^8) for 1 h at 37°C with or without the presence of complement inhibitor DAF (10 μg/ml). Neutrophils were then pelleted at 300 g for 5 min, resuspended, and applied on MLMVECs. After 1 h incubation, non-adherent neutrophils were washed off with HBSS for three times (Chatterjee, Yang, Ma, Cha, et al., 2020). Coverslips were fixed, permeabilized with PBS+0.1% Triton X, and blocked with 10% donkey serum. MLMVECs and neutrophils were labelled with goat anti-mouse ICAM-1 antibody and rat anti-mouse neutrophil antibody respectively overnight at 4°C. After washing three times, donkey-anti-goat AlexaFluor568 and donkey-anti rat AlexaFluor488 were added on the coverslips for 1 h. Prolong Diamond Mounting Medium was used to for nuclei staining and mounting. Images were captured using Leica SP8 Spectral Inverted Laser Scanning Confocal Microscope.

Neutrophil transmigration-—MLMVECs were cultured on 24-well transwell insert to confluence. 100 μl neutrophils (1×10^5) were incubated with 100 μl EVs (~10^8) for 1 h at 37°C with or without the presence of complement inhibitor DAF (10 μg/ml). Neutrophils were then pelleted, resuspended, and added to the top chamber of the transwell plate. f-MLP (10 μM) was then added in the bottom chamber as chemoattractant. After incubation for 1 h at 37°C, the number of transmigrated neutrophils in the bottom chamber were counted in duplicate using hemocytometer (Yang et al., 2018).

NETosis-—neutrophils (1×10^5) were seeded in Costar black clear bottom 96 well plates 30 min prior to treatment. 100 μl of EVs (~10^8) isolated from different groups were then added in duplicate and incubated with neutrophils for 2 h at 37°C. DAF (10 μg/ml) was used as a complement inhibitor. 30 min before the end of incubation, DNAase I and Triton X was added into negative and positive control wells, respectively. Sytox green (1 μM) was added to each well and incubated for 15 min at 37°C. Fluorescence intensity was determined using spectrophotometer at excitation 500 nm and emission 525 nm. Percentage of NETosis was calculated as: $\frac{(Intensity\ of\ the\ well - Intensity\ of\ negative\ control)}{ntensity\ of\ positive\ control} \times 100\%$ (Chatterjee, Yang, Ma, Cha, et al., 2020).

2.12 | Neutrophil infiltration in lungs

Mice were anaesthetized, exsanguinated, and perfusion fixed with 4% paraformaldehyde 24 h after CLP induction. The lungs were excised and inflated with 4% paraformaldehyde. After 24 h of fixation, lungs were processed for paraffin embedding and then sectioned at 5 μm thickness. Sections were de-paraffinized, rehydrated, and stained with hematoxylin and eosin. Images were captured using Keyence BZ-X710 (Itasca, IL, USA). Neutrophils have distinctive multi-lobulated nuclei. The number of neutrophils was then counted.

2.13 | Statistical analysis

See “LC-MS/MS analysis and data processing” section for statistical methods used for proteomics data analysis. All other results are expressed as mean ± SEM and analyzed using GraphPad 7.0. Comparison between two groups were performed using unpaired Student’s *t*-test. Comparison between three groups or more was performed using one-way ANOVA with

Tukey's multiple comparison test. Survival rate was compared using Log-Rank (Mantel-Cox) test. p-Value less than 0.05 was significant.

3 | RESULTS

3.1 | EV isolation and characterization

To investigate the impact of palmitoylation on EVs in response to septic injury, EVs were isolated and characterized as illustrated in Figure 1. Both WT mice and *Zdhhc21*$^{dep/dep}$ mice were subjected to cecal ligation and puncture (CLP)-induced septic injury. Circulating EVs were isolated using ultracentrifugation and purified by size-exclusion chromatography (SEC) (Figure 1a). The amount of EVs (Figure 1b bar graph) and proteins (Figure 1b line graph and Figure 1c) in each SEC fraction indicated that the fractions we collected (fractions 5–9) were enriched in EVs and with minimal contamination of plasma proteins. Western blot confirmed that EV lysates of these fractions were enriched in EV markers CD9 and CD81, but not plasma IgG (Figure 1d). The transmission electron microscopy images in Figure 1e confirmed the presence of EVs and showed the collected EVs are heterogeneous in size. Collectively, these data verified that EVs were selectively isolated from mouse plasma.

3.2 | Inhibiting palmitoylation by DHHC21 functional deficiency attenuates sepsis-induced EV production

We first examined if palmitoylation affects circulating EV profile during sepsis. The number and size of circulating EVs were determined in WT and *Zdhhc21*$^{dep/dep}$ mice subjected to sham or CLP procedure. Both the representative curve (Figure 2a,b) and the quantification data (Figure 2c) of nanoparticle tracking analysis (NTA) showed no significant difference in the level of EVs between WT and *Zdhhc21*$^{dep/dep}$ mice under baseline condition. However, a significant increase in EV production was observed in WT mice after CLP, which was greatly inhibited in *Zdhhc21*$^{dep/dep}$ mice. Moreover, DHHC21 loss-of-function exerted no significant effects on the size of EVs in either sham or CLP-challenged mice (Figure 2d).

3.3 | Proteome profiling of palmitoylated proteins on EVs

To study the effects of palmitoylation on EV content, the cargo of WT and *Zdhhc21*$^{dep/dep}$ EVs were then compared using quantitative proteomic analysis. Palmitoylated proteins on EVs were separated by resin-assisted capture and processed by liquid chromatography with tandem mass spectrometry (LC-MS/MS). A total of 548 palmitoylated proteins were identified from all EV samples with a false discovery rate of 1%. We first crossed check our protein list with palmitoylation database SwissPalm_Mus musculus. Of the 548 identified proteins, 400 proteins have been confirmed as palmitoylated proteins with high confidence according to SwissPalm (Figure 3a). Besides, 148 novel palmitoylated proteins were discovered on EVs. Next, we compared our palmitoyl-protein list with EV database Vesiclepedia_Mus musculus and exosome database Exocarta. Our results revealed that 93% of our identified proteins have been previously reported for their presence on EVs (Figure 3b). Among the top 50 EV makers from Exocarta, 30 EV markers were found in our protein list (Figure 3c). These data reflected the efficacy of our EV isolation and palmitoylated protein separation techniques.

To gain functional insight into the palmitoylated EV proteins, we conducted gene ontology (GO) enrichment analysis using DAVID platform. Our results showed that the identified proteins were mainly enriched in cellular components such as extracellular region, EVs, and extracellular organelles (Supplementary Figure S1), further confirming the purity of the isolated EVs. Panther classification results indicated that the majority of the isolated proteins belonged to defence/immunity proteins (Figure 3d). Consistently, GO biological process enrichment analysis revealed that the most enriched function of our protein list was immune responses (Figure 3e).

3.4 | Inhibition of palmitoylation alters EV palmitoyl-protein profile in mice with septic injury

We then quantitatively compared the palmitoylated EV proteins among groups. As illustrated by the hierarchical clustered heatmap in Figure 4a (Column 1 vs. Column 2), the expression pattern of palmitoylated proteins were similar between WT and *Zdhhc21*$^{dep/dep}$ EVs under baseline condition. Septic injuries remarkably altered the palmitoyl-protein profile of EVs in WT mice (Figure 4a, Column1 vs. Column 3). As shown by the volcano plots in Figure 4b, the levels of 122 palmitoylated proteins on EVs were significantly changed by sepsis in WT mice. Next, we evaluated if DHHC21 deficiency affects EV palmitoyl-protein content during sepsis. Our results in Figure 4a (Column 3 vs. Column 4) indicated that there were profound differences in palmitoyl-proteomes between WT and *Zdhhc21*$^{dep/dep}$ EVs after sepsis. Inhibiting DHHC21-mediated palmitoylation significantly altered the expression of 39 palmitoylated EV proteins upon CLP (Figure 4e). The identity and expression of these proteins were listed in supplementary Table S2 and S3.

3.5 | Septic injury results in increased production of complement enriched EVs

To study the effects of septic injury on EV cargo content, further analyses were performed on the differently expressed palmitoylated EV proteins between sham and CLP-treated WT mice. Principal component analysis (PCA) showed that WT EV data of septic mice clustered together and segregated away from that of control mice (Figure 5a), further confirming distinct palmitoyl-protein profiles between these two groups. We then performed functional analysis on CLP-altered EV palmitoylated proteins. Our disease enrichment results indicated that a significant portion of CLP-altered EV palmitoylated proteins were associated with sepsis, bacterial infections, and acute infectious diseases (Supplementary Figure S2), which suggests that EV palmitoyl-proteome can accurately reflect the pathological states of the mice. GO biological process enrichment analysis further revealed that these proteins were strongly enriched in innate immune response and complement activation (Figure 5b).

In addition to identifying the involved biological functions in response to septic injury, we also assessed whether these functions were activated or inhibited using ingenuity pathway analysis (IPA) prediction. CLP-altered palmitoylated proteins were analyzed via IPA Disease and Function. As shown in Figure 5c, a number of biological functions were predicted to be activated in EVs after sepsis, including inflammation response, immune cell trafficking, and cell-cell interaction. Of all the activated functions, complement activation ranked the highest in statistical significance with a *p*-value of 2.57× E-23. IPA Network Display image in Figure 5d revealed CLP-induced changes in the expression of key complement factors on

WT EVs. The protein names, log2 value, and p-values were listed in Supplementary Table S4. More importantly, the complement pathway was predicted to be activated in EVs from CLP-challenged WT mice.

3.6 | Blocking palmitoylation via DHHC21 loss-of-function attenuates sepsis-induced complement activation in EVs

Next, we studied the impact of palmitoylation on EV cargos by examining differently expressed palmitoylated proteins between WT and *Zdhhc21*$^{dep/dep}$ EVs after CLP. Our IPA results in Figure 6a indicated that DHHC21 loss-of-function attenuated sepsis-mediated activation of biological functions such as inflammation response, immune cell trafficking, and cell-cell interaction. GO biological process enrichment analysis revealed that complement activation function was affected the most by DHHC21 functional deficiency (Figure 6b). Figure 6c summarized DHHC21 functional deficiency-caused expressional changes in complement components on EVs under septic inflammation. The majority of complement components of all three pathways were decreased in *Zdhhc21*$^{dep/dep}$ EVs compared to WT EVs after CLP. Among them, C3 in classical and lectin pathway, mannan-binding lectin serine protease 1 and 2 (MASP-1,-2) in lectin pathway, and complement factor B (CFB) in alternative pathway were significantly downregulated by DHHC21 functional deficiency. IPA predication in Figure 6d confirmed that the complement pathways were inhibited in *Zdhhc21*$^{dep/dep}$ EVs compared to WT EVs after CLP. The complement component names, log2 value, and *p*-values were listed in Supplementary Table S5.

3.7 | Inhibition of palmitoylation via DHHC21 functional deficiency blocks EV-induced neutrophil activation and improves survival after CLP

We then moved on to investigate whether DHHC21-mediated changes in EV cargos affected the function of EVs. Our previous study has revealed that EVs generated under inflammatory condition promoted neutrophil activation (Chatterjee, Yang, Ma, Cha, et al., 2020). We first compared the effects of WT and *Zdhhc21*$^{dep/dep}$ EVs on neutrophil adhesion. As shown in Figure 7a,b, EVs from WT mice after CLP increased neutrophil adhesion to TNF-α pre-stimulated mouse lung microvascular endothelial cells (MLMVECs). This effect was greatly inhibited by decay-accelerating factor (DAF), a complement inhibitor that inhibits all three complement cascades by interfering with C3 and C5 convertases. (Brodbeck et al., 2000) *Zdhhc21*$^{dep/dep}$ EVs, which contained reduced complement components compared to WT EVs after sepsis, were less capable of promoting neutrophil adhesion.

For neutrophil transmigration assay, EV-pretreated neutrophils were applied onto MLMVEC monolayer in Transwell plates (Figure 7c). Compared to EVs from control mice, EVs from CLP-challenged WT mice enhanced N-formyl-methionyl-leucyl-phenylalanine (fMLP)-induced neutrophil transmigration across MLMVEC monolayer. Yet, this increase in neutrophil transmigration was greatly ameliorated by DAF, indicating the involvement of complement system. With less complement components, *Zdhhc21*$^{dep/dep}$ EVs from septic mice displayed reduced ability to induce neutrophil transmigration compared to WT EVs from septic mice.

Emerging evidence has demonstrated that complement activation induces neutrophil extracellular trap (NET) formation (De Bont et al., 2019; Yipp et al., 2012). Given that DHHC21 loss-of-function inhibited sepsis-caused complement activation on EVs, we tested if blocking DHHC21-mediated palmitoylation affects EV-induced NET formation. As illustrated in Figure 7d, significantly increased neutrophils produced NETs upon treating with WT EVs from CLP-treated mice; the effect was blocked by complement inhibitor DAF. Moreover, *Zdhhc21*$^{dep/dep}$ EVs from CLP-treated mice displayed blunted NET-inducing effects compared to WT EVs from CLP-treated mice. These data suggested that *Zdhhc21*$^{dep/dep}$ EVs from septic mice are less capable of inducing neutrophil activation than WT EVs from septic mice, which is, at least partly, due to the reduced complement components on EVs caused by DHHC21 loss-of-function. Consistently, our *in vivo* study indicated that mice with DHHC21 deficiency exhibited significantly less neutrophil infiltration in lungs after septic injury compared to WT mice (Figure 7e,f). Also, *Zdhhc21*$^{dep/dep}$ mice were more resistant to CLP-induced mortality (Figure 7g).

4 | DISCUSSION

In the present study, we demonstrate palmitoylation as a novel regulatory mechanism for EV production, cargo composition, and function. To the best of our knowledge, we are the first to investigate the functional impact of palmitoylation on EVs during sepsis. Our findings indicate that DHHC21 functional deficiency inhibits sepsis-induced increase in plasma EVs. We show that *Zdhhc21*$^{dep/dep}$ EVs display less complement components compared to WT EVs after CLP, which is, at least partly, responsible for the attenuated ability of *Zdhhc21*$^{dep/dep}$ EVs to activate neutrophils. Our *in vivo* results show reduced neutrophil infiltration to the lungs and decreased mortality in *Zdhhc21*$^{dep/dep}$ mice after CLP. This study also provides the first comprehensive palmitoyl-proteomic profiling of circulating EVs in response to sepsis, where the majority of palmitoylated proteins are identified as proinflammatory molecules. Our dataset may be used as one of the few available resources for further investigation of palmitoylated EV cargos.

Since the first electron microscope image showing the existence of EVs (Aaronson et al., 1971), there has been an exponentially increasing interest in EVs with respect to their production and function in various pathophysiological states. Elevated levels of circulating EVs have been reported in patients with infectious diseases, immune disorders, and cancer (Aharon et al., 2014; Pando et al., 2018). Our results indicate that the number of circulating EVs increases after CLP-induced septic injury. In line with our finding, increased plasma EVs have been reported in patients with sepsis compared to healthy controls (Stiel et al., 2016; Zhang et al., 2016). Patients with septic shock display higher circulating EVs than septic patients without shock (Im et al., 2020). Moreover, the level of circulating EVs is positively associated with Sequential Organ Failure Assessment (SOFA) score and 28-day mortality (Im et al., 2020).

Emerging evidence indicates that circulating EVs not only serve as biomarkers, but also function as pathological mediators in disease propagation and organ injuries. Circulating EVs transfer a large number of bioactive substances or signalling molecules to neighbouring and distant cells through endocytosis or membrane fusion, where they rapidly alter the

function and fate of recipient cells (Rontogianni et al., 2019). For example, it has been reported that caspase-1 containing EVs in patients with sepsis induce apoptosis of target cells (Exline et al., 2014). Our recent study shows that plasma EVs deliver tyrosine kinase c-Src to endothelial cells (ECs) causing EC barrier dysfunction during inflammation (Chatterjee, Yang, Ma, Cha, et al., 2020). Other studies have reported that EVs are capable of mediating inflammation and triggering immune cell activation (Vats et al., 2020; X. Zhou et al., 2020). For instance, macrophage-derived EVs activate naïve macrophages, resulting in increased chemokine release (Zhang et al., 2019). In line with this, our current data show that EVs collected from CLP-challenged mice are capable of enhancing neutrophil adhesion, transmigration, and NET formation. Similar neutrophil-activating effects of EVs have also been reported in other inflammatory settings by us and other groups (Chatterjee, Yang, Ma, Cha, et al., 2020; Walters et al., 2019).

Given the pathological roles of EVs in sepsis, it is of great importance to understand the regulatory mechanism underlying EV production during sepsis. Our previous results show drastically increased palmitoylation in cells under inflammatory conditions (Beard et al., 2016). To test the contribution of palmitoylation to sepsis-induced EV production in vivo, we used mice with DHHC21 functional deficiency resulting from a 3 bp deletion in exon 7 of *Zdhhc21* gene (Beard et al., 2016; Yang et al., 2021). DHHC21 is primarily expressed on plasma membrane, which is different from the majority of other DHHCs that are localized in endoplasmic reticulum and/or Golgi apparatus. Plasma membrane plays critical roles in EV biogenesis: early endosomes are formed by invagination of plasma membrane; small EV release requires the docking and fusion of MVBs with plasma membrane; the formation of large EVs relies on the outward budding and pinching of plasma membrane (Russell et al., 2019). The plasma membrane localization of DHHC21 may allow DHHC21 to regulate many aspects of EV formation. This hypothesis is supported by our results showing that inhibition of DHHC21-mediated palmitoylation reduces plasma EVs. Specific EV subpopulation may respond differently than total EV numbers. A previous *in vitro* study has reported that treatment of skeletal muscle cells with 2-bromopalmitate (2-BP), a general inhibitor of DHHCs, results in increased production of small EVs (<150 nm) (Romancino et al., 2018). This seemingly opposite finding may be due to the fact that only a small subpopulation of EVs were included for measurement and that the off-target effects of 2-BP may also affect EV production.

Inhibition of palmitoylation may regulate sepsis-induced EV production through multifaced mechanisms. EV biogenesis requires an orchestration of multiple membrane-associated proteins such as tetraspanins, ESCRTs, and small GTPases. Altering the palmitoylation status of these proteins could affect their membrane localization, conformation, and ability to interact with other proteins (Yang et al., 2020). For example, tetraspanins are well-established palmitoylation substrates that can change the curvature of membranes and interact with cytoskeletal proteins to facilitate membrane budding and EV formation (Bari et al., 2011; Sala-Valdés et al., 2006; Umeda et al., 2020). Inhibiting the palmitoylation of tetraspanins disrupts not only their membrane localization but also their interaction with other tetraspanins and proteins, greatly impairing their functions. In addition, the Rab and Rac small GTPase families, which control MVB fusion with plasma membrane, also undergo palmitoylation-mediated regulation (Homma et al., 2021; Modica& Lefrancois,

2020; Modica et al., 2017). Non-palmitoylated small GTPases such as Rac have been reported to exhibit decreased GTP loading rate and reduced enzymatic activity (Navarro-Lérida et al., 2012). Besides, the functional impacts of palmitoylation have been shown for proteins such as ESCRT-associated protein Alix, phospholipase D, and flotillins, all are key participants in EV biogenesis (Kwiatkowska et al., 2020; Romancino et al., 2018; Yin et al., 2010).

In addition to the number of EVs, EV cargo content is also affected by palmitoylation through both direct and indirect ways. Previous reports have shown that palmitoylation directly targets modified proteins into secreted vesicles via lipophilic interaction-mediated membrane anchorage (Fang et al., 2007). Besides, palmitoylation regulates EV content selection through protein-protein interaction. For instance, inhibition of palmitoylation blocks the binding of Alix and CD9, resulting in reduced CD9 level in EVs (Romancino et al., 2018). Similarly, our proteomic analysis and IPA results demonstrate that reduced palmitoylation in DHHC21 loss-of-function attenuates sepsis-induced increase of complement components in EVs. More specifically, compared to WT EVs from CLP-challenged mice, the levels of C3, MASP-1, MASP-2, and CFB are significantly decreased in *Zdhhc21*$^{dep/dep}$ EVs.

EV cargo content is an important determinant of their effects on target cells. Several studies have shown that EVs regulate immune responses via the complement components carried by them. For example, C1q, C3, and C4 in leukocyte-derived EVs have been reported to activate innate immune responses (Biro et al., 2007; Karasu et al., 2018). In contrast, EVs derived from tumour cells are enriched in complement factor H, which suppresses the immune responses against tumour tissues (Mao et al., 2020). Our results utilizing complement inhibitor also suggest that complements in EVs contribute to EV-induced neutrophil activation. Compared to EVs from wildtype mice after CLP challenge, EVs from *Zdhhc21*$^{dep/dep}$ mice after CLP challenge contained reduced complement components and exhibit decreased ability to activate neutrophils. The responsible complement components on EVs may include, but are not limited to C3a, C5a, and C5b-9 (Camous et al., 2011). Furthermore, inhibiting EV-induced neutrophil activation by DHHC21 deficiency may exert protective effects in mice subjected to CLP challenges, as evidenced by reduced neutrophil recruitment to lungs and improved survival, suggesting the therapeutic potential of regulating EV function by palmitoylation in combating septic injuries.

It is noteworthy that CLP induces the upregulation/activation of other inflammatory-related pathways in circulating EVs (Supplementary Figure S3), which are attenuated in DHHC21 loss-of-function. These alterations may also contribute to EV-mediated neutrophil activation. While it is not practical to investigate every potential mechanism in this study, we select the complement pathway for further analysis, as it is the most activated function after septic injury and is most significantly affected by DHHC21. In addition, it is likely that increased complement components in EVs may exert other effects, such as endothelial dysfunction and thrombosis (Afshar-Kharghan, 2017; Fischetti & Tedesco, 2006), which can be studied in future. Likewise, the current study is focused on the changes in total EVs without differentiating EV subtypes or cellular origins. Sepsis triggers massive EV shedding from various types of cells. It has been demonstrated that the majority of the EVs released

during sepsis are derived from platelets and innate immune cells (Raeven et al., 2018). In future studies, we will identify the precise EV sources and investigate the specific effects of palmitoylation on individual EV subtypes.

In summary, the present study provides the first line of evidence supporting a critical role of palmitoylation in regulating EV production and cargo composition during septic injury. Loss-of-function in DHHC21-mediated palmitoylation suppresses sepsis-induced increases in circulating EVs and their function to activate neutrophils involving a complement-related pathway.

Supplementary Material

Refer to Web version on PubMed Central for supplementary material.

ACKNOWLEDGEMENTS

This work was supported by NIH grants R35 HL150732 (to SYY), R01 GM142110 (to SYY and MHW), Department of Veterans Affairs grants I01BX000799 and IK6BX004210 (to MHW), and Shock Society Faculty Research Award (to XY). We thank Weill Cornell Medicine Proteomics and Metabolomics Core Facility for proteomic analysis.

Funding information

Shock Society Faculty Research Award (to XY); National Institutes of Health: R35 HL150732 (to SYY): R01 GM142110 (to SYY and MHW); U.S. Department of Veterans Affairs: I01BX000799: IK6BX004210 (to MHW)

REFERENCES

Aaronson S, Behrens U, Orner R, & Haines TH (1971). Ultrastructure of intracellular and extracellular vesicles, membranes, and myelin figures produced by Ochromonas danica. Journal of Ultrastructure Research, 35(5), 418–430. [PubMed: 4111037]

Abels ER, & Breakefield XO (2016). Introduction to extracellular vesicles: Biogenesis, RNA cargo selection, content, release, and uptake. Cellular and Molecular Neurobiology, 36(3), 301–312. [PubMed: 27053351]

Afshar-Kharghan V (2017). Complement and clot. Blood, 129(16), 2214–2215.. [PubMed: 28428238]

Aharon A, Rebibo-Sabbah A, Tzoran I, & Levin C (2014). Extracellular vesicles in hematological disorders. Rambam Maimonides Medical Journal, 5(4), e0032. [PubMed: 25386348]

Andreu Z, & Yáñez-Mó M (2014). Tetraspanins in extracellular vesicle formation and function. Frontiers in Immunology, 5, 442. [PubMed: 25278937]

Bari R, Guo Q, Xia B, Zhang YH, Giesert EE, Levy S, Zheng JJ, & Zhang XA (2011). Tetraspanins regulate the protrusive activities of cell membrane. Biochemical and Biophysical Research Communications, 415(4), 619–626. [PubMed: 22079629]

Bastin G, & Heximer SP (2013). Rab family proteins regulate the endosomal trafficking and function of RGS4. Journal of Biological Chemistry, 288(30), 21836–21849. [PubMed: 23733193]

Beard RS, Yang X, Meegan JE, Overstreet JW, Yang CGY, Elliott JA, Reynolds JJ, Cha BJ, Pivetti CD, Mitchell DA, Wu MH, Deschenes RJ, & Yuan SY (2016). Palmitoyl acyltransferase DHHC21 mediates endothelial dysfunction in systemic inflammatory response syndrome. Nature Communication, 7, 12823.

Biro E, Nieuwland R, Tak PP, Pronk LM, Schaap MCL, Sturk A, & Hack CE (2007). Activated complement components and complement activator molecules on the surface of cell-derived microparticles in patients with rheumatoid arthritis and healthy individuals. Annals of the Rheumatic Diseases, 66(8), 1085–1092. [PubMed: 17261534]

Böing AN, Van Der Pol E, Grootemaat AE, Coumans FAW, Sturk A, & Nieuwland R (2014). Single-step isolation of extracellular vesicles by size-exclusion chromatography. Journal of Extracellular Vesicles, 3, 23430..

Boukouris S, & Mathivanan S (2015). Exosomes in bodily fluids are a highly stable resource of disease biomarkers. Proteomics. Clinical Applications, 9(3–4), 358–367. [PubMed: 25684126]

Brodbeck WG, Kuttner-Kondo L, Mold C,& Medof ME (2000). Structure/function studies of human decay-accelerating factor. Immunology, 101(1), 104–111. [PubMed: 11012760]

Camous L, Roumenina L, Bigot S, Brachemi S, Frémeaux-Bacchi V, Lesavre P, & Halbwachs-Mecarelli L (2011). Complement alternative pathway acts as a positive feedback amplification of neutrophil activation. Blood, 117(4), 1340–1349. [PubMed: 21063021]

Carnino JM, Ni K, & Jin Y (2020). Post-translational modification regulates formation and cargo-loading of extracellular vesicles. Frontiers in Immunology, 11, 948. [PubMed: 32528471]

Chatterjee V, Yang X, Ma Y, Cha B, Meegan JE, Wu M,& Yuan SY (2020). Endothelial microvesicles carrying Src-rich cargo impair adherens junction integrity and cytoskeleton homeostasis. Cardiovascular Research, 116(8), 1525–1538. [PubMed: 31504252]

Chatterjee V, Yang X, Ma Y, Wu MH, & Yuan SY (2020). Extracellular vesicles: New players in regulating vascular barrier function. American Journal of Physiology. Heart and Circulatory Physiology, 319(6), H1181–H1196. [PubMed: 33035434]

Clement E, Lazar I, Attané C, Carrié L, Dauvillier S, Ducoux-Petit M, Esteve D, Menneteau T, Moutahir M, Le Gonidec S, Dalle S, Valet P, Burlet-Schiltz O, Muller C, & Nieto L (2020). Adipocyte extracellular vesicles carry enzymes and fatty acids that stimulate mitochondrial metabolism and remodeling in tumor cells. Embo Journal, 39(3), e102525. [PubMed: 31919869]

Cocozza F, Grisard E, Martin-Jaular L, Mathieu M, & Théry C (2020). SnapShot: Extracellular vesicles. Cell, 182(1), 262–262.e1.. [PubMed: 32649878]

Crewe C, Joffin N, Rutkowski JM, Kim M, Zhang F, Towler DA, Gordillo R, & Scherer PE (2018). An endothelial-to-adipocyte extracellular vesicle axis governed by metabolic state. Cell, 175(3), 695–708.e13.. [PubMed: 30293865]

De Abreu RC, Fernandes H, Da Costa Martins PA, Sahoo S, Emanueli C, & Ferreira L (2020). Native and bioengineered extracellular vesicles for cardiovascular therapeutics. Nature Reviews Cardiology, 17(11), 685–697. [PubMed: 32483304]

De Bont CM, Boelens WC, & Pruijn GJM (2019). NETosis, complement, and coagulation: A triangular relationship. Cellular & Molecular Immunology, 16(1), 19–27. [PubMed: 29572545]

Exline MC, Justiniano S, Hollyfield JL, Berhe F, Besecker BY, Das S, Wewers MD, & Sarkar A (2014). Microvesicular caspase-1 mediates lymphocyte apoptosis in sepsis. PLoS One, 9(3), e90968. [PubMed: 24643116]

Fan Y, Shayahati B, Tewari R, Boehning D, & Akimzhanov AM (2020). Regulation of T cell receptor signaling by protein acyltransferase DHHC21. Molecular Biology Reports, 47(8), 6471–6478. [PubMed: 32789573]

Fang Y, Wu N, Gan X, Yan W, Morrell JC, & Gould SJ (2007). Higher-order oligomerization targets plasma membrane proteins and HIV gag to exosomes. PLoS Biology, 5(6), e158. [PubMed: 17550307]

Fischetti F, & Tedesco F (2006). Cross-talk between the complement system and endothelial cells in physiologic conditions and in vascular diseases. Autoimmunity, 39(5), 417–428. [PubMed: 16923542]

Hessvik NP, & Llorente A (2018). Current knowledge on exosome biogenesis and release. Cellular and Molecular Life Sciences, 75(2), 193–208. [PubMed: 28733901]

Homma Y, Hiragi S, & Fukuda M (2021). Rab family of small GTPases: An updated view on their regulation and functions. FEBS Journal, 288(1), 36–55. [PubMed: 32542850]

Hoshino A, Kim HS, Bojmar L, Gyan KE, Cioffi M, Hernandez J, Zambirinis CP, Rodrigues G, Molina H, Heissel S, Mark MT, Steiner L, Benito-Martin A, Lucotti S, Di Giannatale A, Offer K, Nakajima M, Williams C, Nogués L, …, Lyden, D. (2020). Extracellular vesicle and particle biomarkers define multiple human cancers. Cell, 182(4), 1044–1061.e18.. [PubMed: 32795414]

Im Y, Yoo H, Lee JY, Park J, Suh GY, & Jeon K (2020). Association of plasma exosomes with severity of organ failure and mortality in patients with sepsis. Journal of Cellular and Molecular Medicine, 24(16), 9439–9445. [PubMed: 32639098]

Jung MK, & Mun JY (2018). Sample preparation and imaging of exosomes by transmission electron microscopy. Journal of Visualized Experiments: JoVE, 131, 56482..

Kalluri R, & Lebleu VS (2020). The biology, function, and biomedical applications of exosomes. Science, 367(6478), eaau6977.. [PubMed: 32029601]

Karasu E, Eisenhardt SU, Harant J,& Huber-Lang M (2018). Extracellular Vesicles: Packages sent with complement. Frontiers in Immunology, 9, 721. [PubMed: 29696020]

Konoshenko MY, Lekchnov EA, Vlassov AV, & Laktionov PP (2018). Isolation of extracellular vesicles: General methodologies and latest trends. BioMed Research International, 2018, 8545347.. [PubMed: 29662902]

Krämer A, Green J, Pollard J, & Tugendreich S (2014). Causal analysis approaches in Ingenuity Pathway Analysis. Bioinformatics, 30(4), 523–530. [PubMed: 24336805]

Kwiatkowska K, Matveichuk OV, Fronk J, & Ciesielska A (2020). Flotillins: At the intersection of protein S-palmitoylation and lipid-mediated signaling. International Journal of Molecular Sciences, 21(7), 2283.. [PubMed: 32225034]

Manier S, Liu C-J, Avet-Loiseau H, Park J, Shi J, Campigotto F, Salem KZ, Huynh D, Glavey SV, Rivotto B, Sacco A, Roccaro AM, Bouyssou J, Minvielle S, Moreau P, Facon T, Leleu X, Weller E, Trippa L, & Ghobrial IM (2017). Prognostic role of circulating exosomal miRNAs in multiple myeloma. Blood, 129(17), 2429–2436. [PubMed: 28213378]

Mao X, Zhou L, Tey SK, Ma APY, Yeung CLS, Ng TH, Wong SWK, Liu BHM, Fung YME, Patz EF, Cao P, Gao Y, & Yam JWP (2020). Tumour extracellular vesicle-derived Complement Factor H promotes tumorigenesis and metastasis by inhibiting complement-dependent cytotoxicity of tumour cells. Journal of Extracellular Vesicles, 10(1), e12031. [PubMed: 33708358]

Mariscal J, Vagner T, Kim M, Zhou B, Chin A, Zandian M, Freeman MR, You S, Zijlstra A, Yang W, & Di Vizio D (2020). Comprehensive palmitoyl-proteomic analysis identifies distinct protein signatures for large and small cancer-derived extracellular vesicles. Journal of Extracellular Vesicles, 9(1), 1764192. [PubMed: 32944167]

Modica G, & Lefrancois S (2020). Post-translational modifications: How to modulate Rab7 functions. Small GTPases, 11(3), 167–173. [PubMed: 29099291]

Modica G, Skorobogata O, & Sauvageau E, Vissa A, Yip CM, Kim PK, Wurtele H, & Lefrancois S (2017). Rab7 palmitoylation is required for efficient endosome-to-TGN trafficking. Journal of Cell Science, 130(15), 2579–2590. [PubMed: 28600323]

Navarro-Lérida I, Sánchez-Perales S, Calvo M, Rentero C, Zheng Y, Enrich C, & Del Pozo MA (2012). A palmitoylation switch mechanism regulates Rac1 function and membrane organization. EMBO Journal, 31(3), 534–551. [PubMed: 22157745]

Pando A, Reagan JL, Quesenberry P, & Fast LD (2018). Extracellular vesicles in leukemia. Leukemia Research, 64, 52–60. [PubMed: 29190514]

Pegtel DM, & Gould SJ (2019). Exosomes. Annual Review of Biochemistry, 88, 487–514.

Raeven P, Zipperle J, & Drechsler S (2018). Extracellular vesicles as markers and mediators in sepsis. Theranostics, 8(12), 3348–3365. [PubMed: 29930734]

Robbins PD, Dorronsoro A, & Booker CN (2016). Regulation of chronic inflammatory and immune processes by extracellular vesicles. Journal of Clinical Investigation, 126(4), 1173–1180. [PubMed: 27035808]

Romancino DP, Buffa V, Caruso S, Ferrara I, Raccosta S, Notaro A, Campos Y, Noto R, Martorana V, Cupane A, Giallongo A, D'azzo A, Manno M, & Bongiovanni A (2018). Palmitoylation is a post-translational modification of Alix regulating the membrane organization of exosome-like small extracellular vesicles. Biochim Biophys Acta Gen Subj, 1862(12), 2879–2887. [PubMed: 30251702]

Rontogianni S, Synadaki E, Li B, Liefaard MC, Lips EH, Wesseling J, Wu W, & Altelaar M (2019). Proteomic profiling of extracellular vesicles allows for human breast cancer subtyping. Communications Biology, 2, 325. [PubMed: 31508500]

Russell AE, Sneider A, Witwer KW, Bergese P, Bhattacharyya SN, Cocks A, Cocucci E, Erdbrügger U, Falcon-Perez JM, Freeman DW, Gallagher TM, Hu S, Huang Y, Jay SM, Kano S-I, Lavieu G, Leszczynska A, Llorente AM, Lu Q, …, Vader P (2019). Biological membranes in EV biogenesis, stability, uptake, and cargo transfer: An ISEV position paper arising from the ISEV membranes and EVs workshop. Journal of Extracellular Vesicles, 8(1), 1684862. [PubMed: 31762963]

Sala-Valdés M, Ursa Á, Charrin S, Rubinstein E, Hemler ME, Sánchez-Madrid F, & Yáñez-Mó M (2006). EWI-2 and EWI-F link the tetraspanin web to the actin cytoskeleton through their direct association with ezrin-radixin-moesin proteins. Journal of Biological Chemistry, 281(28), 19665–19675. [PubMed: 16690612]

Sharma C, Yang XH, & Hemler ME (2008). DHHC2 affects palmitoylation, stability, and functions of tetraspanins CD9 and CD151. Molecular Biology of the Cell, 19(8), 3415–3425. [PubMed: 18508921]

Shen B, Wu N, Yang J-M, & Gould SJ (2011). Protein targeting to exosomes/microvesicles by plasma membrane anchors. Journal of Biological Chemistry, 286(16), 14383–14395. [PubMed: 21300796]

Stiel L, Delabranche X, Galoisy A-C, Severac F, Toti F, Mauvieux L, Meziani F, & Boisramé-Helms J (2016). Neutrophil fluorescence: A new indicator of cell activation during septic shock-induced disseminated intravascular coagulation. Critical Care Medicine, 44(11), e1132–e1136. [PubMed: 27441905]

Teng F, & Fussenegger M (2020). Shedding light on extracellular vesicle biogenesis and bioengineering. Adv Sci (Weinh), 8(1), 2003505. [PubMed: 33437589]

Théry C, Witwer KW, Aikawa E, Alcaraz MJ, Anderson JD, Andriantsitohaina R, Antoniou A, Arab T, Archer F, Atkin-Smith GK, Ayre DC, Bach J-M, Bachurski D, Baharvand H, Balaj L, Baldacchino S, Bauer NN, Baxter AA, Bebawy M, …, Zuba-Surma EK (2018). Minimal information for studies of extracellular vesicles 2018 (MISEV2018): A position statement of the International Society for Extracellular Vesicles and update of the MISEV2014 guidelines. Journal of Extracellular Vesicles, 7(1), 1535750. [PubMed: 30637094]

Umeda R, Satouh Y, Takemoto M, Nakada-Nakura Y, Liu K, Yokoyama T, Shirouzu M, Iwata S, Nomura N, Sato K, Ikawa M, Nishizawa T,& Nureki O (2020). Structural insights into tetraspanin CD9 function. Nature Communication, 11(1), 1606.

Vats R, Brzoska T, Bennewitz MF, Jimenez MA, Pradhan-Sundd T, Tutuncuoglu E, Jonassaint J, Gutierrez E, Watkins SC, Shiva S, Scott MJ, Morelli AE, Neal MD, Kato GJ, Gladwin MT, & Sundd P (2020). Platelet extracellular vesicles drive inflammasome-IL-1beta-dependent lung injury in sickle cell disease. American Journal of Respiratory and Critical Care Medicine, 201(1), 33–46. [PubMed: 31498653]

Verweij FJ, De Heus C, Kroeze S, Cai H, Kieff E, Piersma SR, Jimenez CR, Middeldorp JM, & Pegtel DM (2015). Exosomal sorting of the viral oncoprotein LMP1 is restrained by TRAF2 association at signalling endosomes. Journal of Extracellular Vesicles, 4, 26334. [PubMed: 25865256]

Vestad B, Llorente A, Neurauter A, Phuyal S, Kierulf B, Kierulf P, Skotland T, Sandvig K, Haug KBF, & Øvstebø R (2017). Size and concentration analyses of extracellular vesicles by nanoparticle tracking analysis: A variation study. Journal of Extracellular Vesicles, 6(1), 1344087. [PubMed: 28804597]

Vietri M, Radulovic M, & Stenmark H (2020). The many functions of ESCRTs. Nature Reviews Molecular Cell Biology, 21(1), 25–42. [PubMed: 31705132]

Walters N, Nguyen LTH, Zhang J, Shankaran A, & Reátegui E (2019). Extracellular vesicles as mediators of in vitro neutrophil swarming on a large-scale microparticle array. Lab on A Chip, 19(17), 2874–2884. [PubMed: 31343025]

Wen C, Seeger RC, Fabbri M, Wang L, Wayne AS, & Jong AY (2017). Biological roles and potential applications of immune cell-derived extracellular vesicles. Journal of Extracellular Vesicles, 6(1), 1400370. [PubMed: 29209467]

Xu R, Rai A, Chen M, Suwakulsiri W, Greening DW, & Simpson RJ (2018). Extracellular vesicles in cancer - implications for future improvements in cancer care. Nature Reviews Clinical Oncology, 15(10), 617–638.

Yang X, Chatterjee V, Ma Y, Zheng E, & Yuan SY (2020). Protein palmitoylation in leukocyte signaling and function. Frontiers in Cell and Developmental Biology, 8, 600368. [PubMed: 33195285]

Yang X, Meegan JE, Jannaway M, Coleman DC, & Yuan SY (2018). A disintegrin and metalloproteinase 15-mediated glycocalyx shedding contributes to vascular leakage during inflammation. Cardiovascular Research, 114(13), 1752–1763. [PubMed: 29939250]

Yang X, Zheng E, Ma Y, Chatterjee V, Villalba N, Breslin JW, Liu R, Wu MH, & Yuan SY (2021). DHHC21 deficiency attenuates renal dysfunction during septic injury. Science Reports, 11(1), 11146.

Yin H, Gui Y, Du G, Frohman MA, & Zheng X-L (2010). Dependence of phospholipase D1 multi-monoubiquitination on its enzymatic activity and palmitoylation. Journal of Biological Chemistry, 285(18), 13580–13588.. [PubMed: 20189990]

Yipp BG, Petri B, Salina D, Jenne CN, Scott BNV, Zbytnuik LD, Pittman K, Asaduzzaman M, Wu K, Meijndert HC, Malawista SE, De Boisfleury Chevance A, Zhang K, Conly J, & Kubes P (2012). Infection-induced NETosis is a dynamic process involving neutrophil multitasking in vivo. Nature Medicine, 18(9), 1386–1393.

Yu J, Gu X, & Yi S (2016). Ingenuity pathway analysis of gene expression profiles in distal nerve stump following nerve injury: Insights into wallerian degeneration. Frontiers in Cellular Neuroscience, 10, 274. [PubMed: 27999531]

Zhang Y, Jin X, Liang J, Guo Y, Sun G, Zeng X, & Yin H (2019). Extracellular vesicles derived from ODN-stimulated macrophages transfer and activate Cdc42 in recipient cells and thereby increase cellular permissiveness to EV uptake. Science Advances, 5(7), eAav1564. [PubMed: 31355328]

Zhang Y, Meng H, Ma R, He Z, Wu X, Cao M, Yao Z, Zhao L, Li T, Deng R, Dong Z, Tian Y, Bi Y, Kou J, Thatte HS, Zhou J,& Shi J (2016). Circulating microparticles, blood cells, and endothelium induce procoagulant activity in sepsis through phosphatidylserine exposure. Shock (Augusta, Ga.), 45(3), 299–307. [PubMed: 26513704]

Zhou B, Wang Y, Yan Y, Mariscal J, Di Vizio D, Freeman MR,& Yang W (2019). Low-background acyl-biotinyl exchange largely eliminates the coisolation of non-S-acylated proteins and enables deep S-acylproteomic analysis. Analytical Chemistry, 91(15), 9858–9866. [PubMed: 31251020]

Zhou X, Xie F, Wang L, Zhang L, Zhang S, Fang M, & Zhou F (2020). The function and clinical application of extracellular vesicles in innate immune regulation. Cellular & Molecular Immunology, 17(4), 323–334. [PubMed: 32203193]

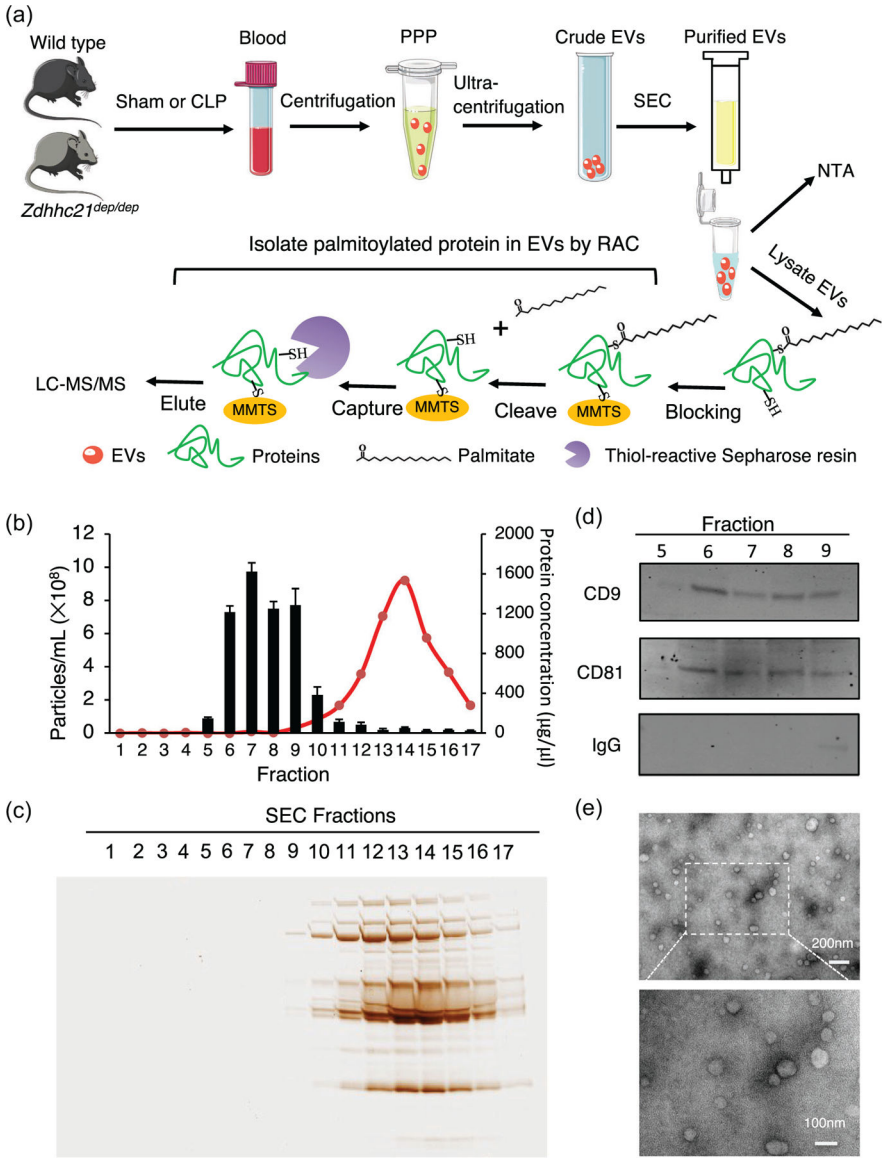

FIGURE. Extracellular vesicle isolation and characterization.

(a) Workflow diagram. WT and *Zdhhc21*$^{dep/dep}$ mice are subjected to sham procedure or CLP-induced septic injury. Mouse blood is collected 24 h after the surgery and centrifuged to generate platelet poor plasma (PPP). Crude EVs are then pelleted by ultracentrifugation of PPP at 100,000 g for 2 h. Size-exclusion chromatography (SEC) is utilized to purify the EVs. The number of EVs is quantified using NTA. Purified EVs are lysed, and palmitoylated proteins in EVs are enriched using Resin-assisted capture. Next, palmitoyl-proteome of EVs is analyzed by LC-MS/MS. Images of mice and tubes were obtained from Smart Servier Medical Art (https://smart.servier.com). (b) The concentration of EVs and proteins in each SEC fraction. EVs (black bars) are measured by NTA, and proteins (red curve) are determined by Bradford assay. Fractions 5–9 are collected for EV isolation. (c) The protein abundance in each SEC fraction is visualized by loading the samples on stain-free SDS-

PAGE gels. (d) The levels of CD9, CD81, and plasma protein IgG in collected fractions. (e) Transmission electron microscopy images showing isolated EVs are heterogeneous in size

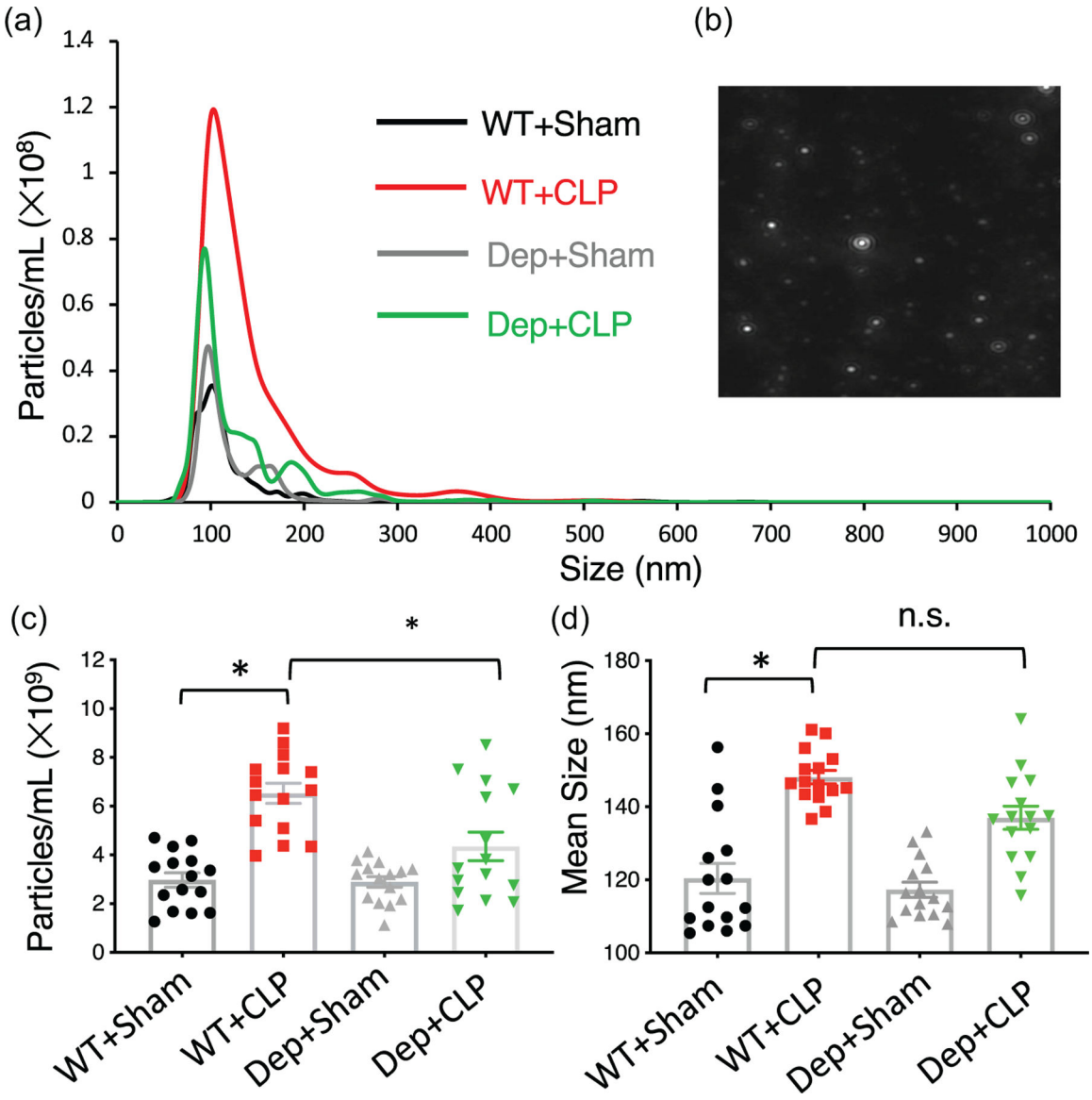

FIGURE 2. DHHC21 loss-of-function inhibits sepsis-induced EV production.

(a) Representative NTA curves showing the size distribution of circulating EVs. The average particle/protein ratio of EV samples is 3.03×10^{10} particles/μg of protein. (b) Representative image showing the EVs detected by NTA. (c) *Zdhhc21*$^{dep/dep}$ mice exhibit reduced number of circulating EVs after CLP compared with WT mice. Results represent mean ± SEM. $n = 15$. (d) Mean size of the EVs determined by NTA. Results represent mean ± SEM. $n = 15$. *$p < 0.05$

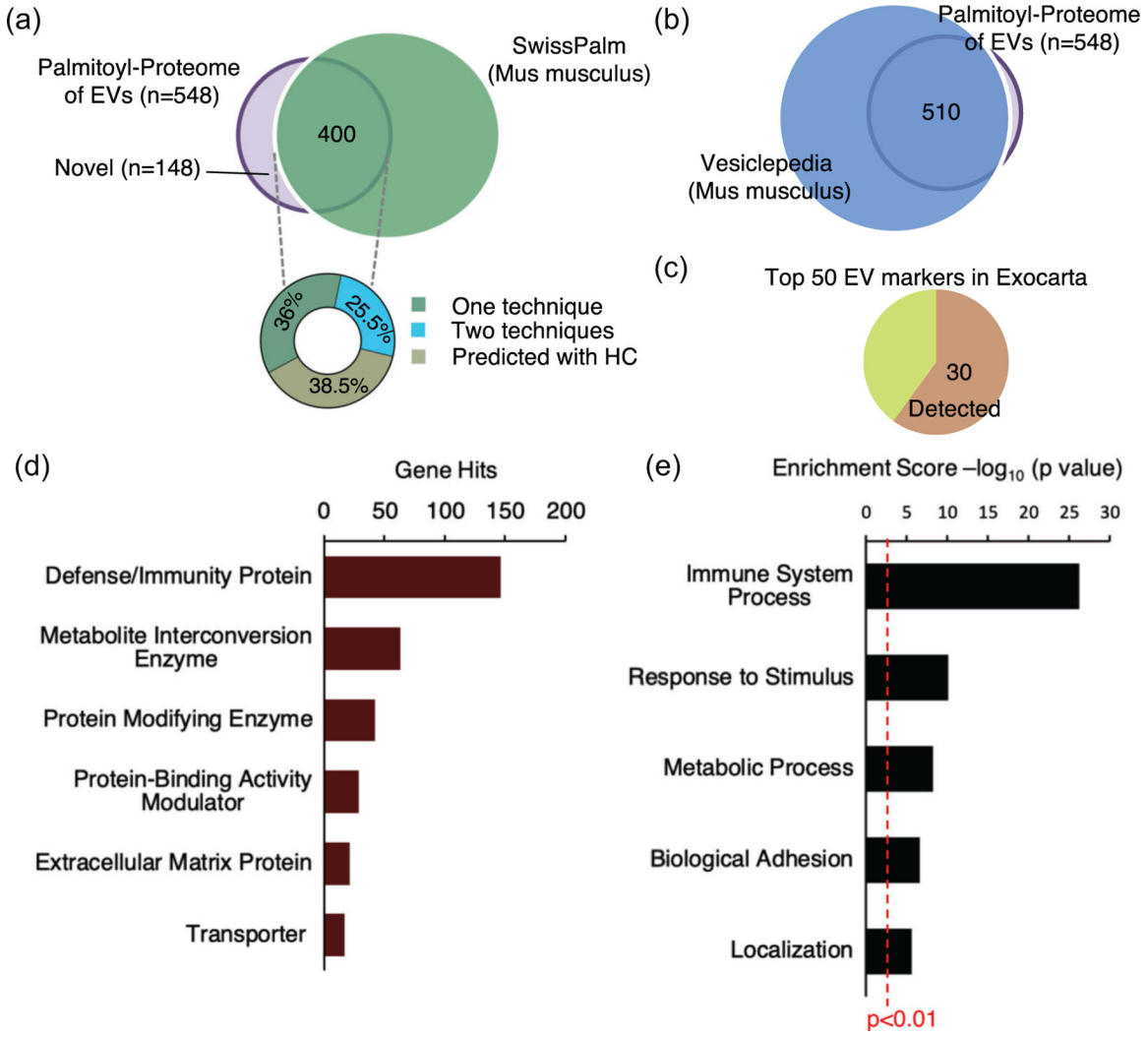

FIGURE 3. EV palmitoyl-protein profile identified by LC-MS/MS.

Twelve samples from four groups (WT+sham, WT+CLP, Dep+sham, and Dep+CLP, $n = 3$ in each group) are quantitively analyzed using LC-MS/MS. A total of 548 high-confidence proteins were identified with a false discovery rate of 1%. (a) Venn diagram showing 400 of the identified EV palmitoylated proteins overlap with SwissPalm_Mouse database. Based on Swisspalm classification, 25.5% of our high-confidence palmitoylated proteins are validated by two different palmitoyl-proteomic techniques; 36% are validated by one palmitoyl-proteomic techniques; 38.5% are predicted to be palmitoylated proteins with high confidence. (b) Venn diagram showing the number of identified proteins in EV samples that overlap with EV database Vesiclepedia_Mus musculus. (c) Pie chart shows that 30 of the top 50 EV markers reported in Exocarta database are detected in our EV palmitoyl-proteome. (d) Protein classification analysis of the EV palmitoyl-proteome using Panther classification system. (e) Gene ontology enrichment biological process analysis of the EV palmitoyl-proteome using DAVID database

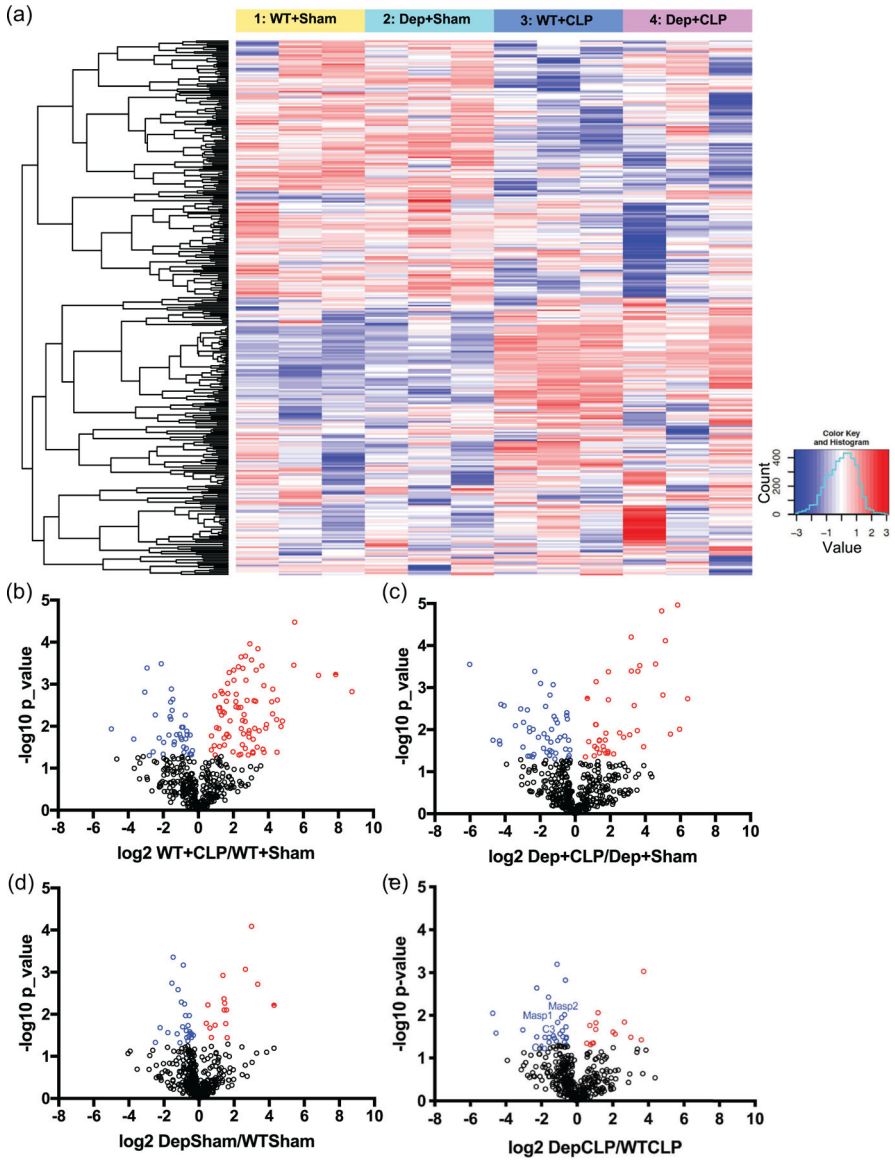

FIGURE 4. WT and *Zdhhc21*$^{dep/dep}$ mice display distinct EV palmitoyl-protein profiles in septic injury.

(a) Hierarchical clustering heatmap shows the palmitoyl-protein profiles of EVs collected from WT and *Zdhhc21*$^{dep/dep}$ mice after sham procedure or CLP. $n = 3$ independent samples for each group. (b–e) Volcano plot showing the significantly altered palmitoylated proteins between the two groups. Upregulated proteins are labelled red; downregulated proteins are labelled blue. $p < 0.05$ is considered as the threshold for significance

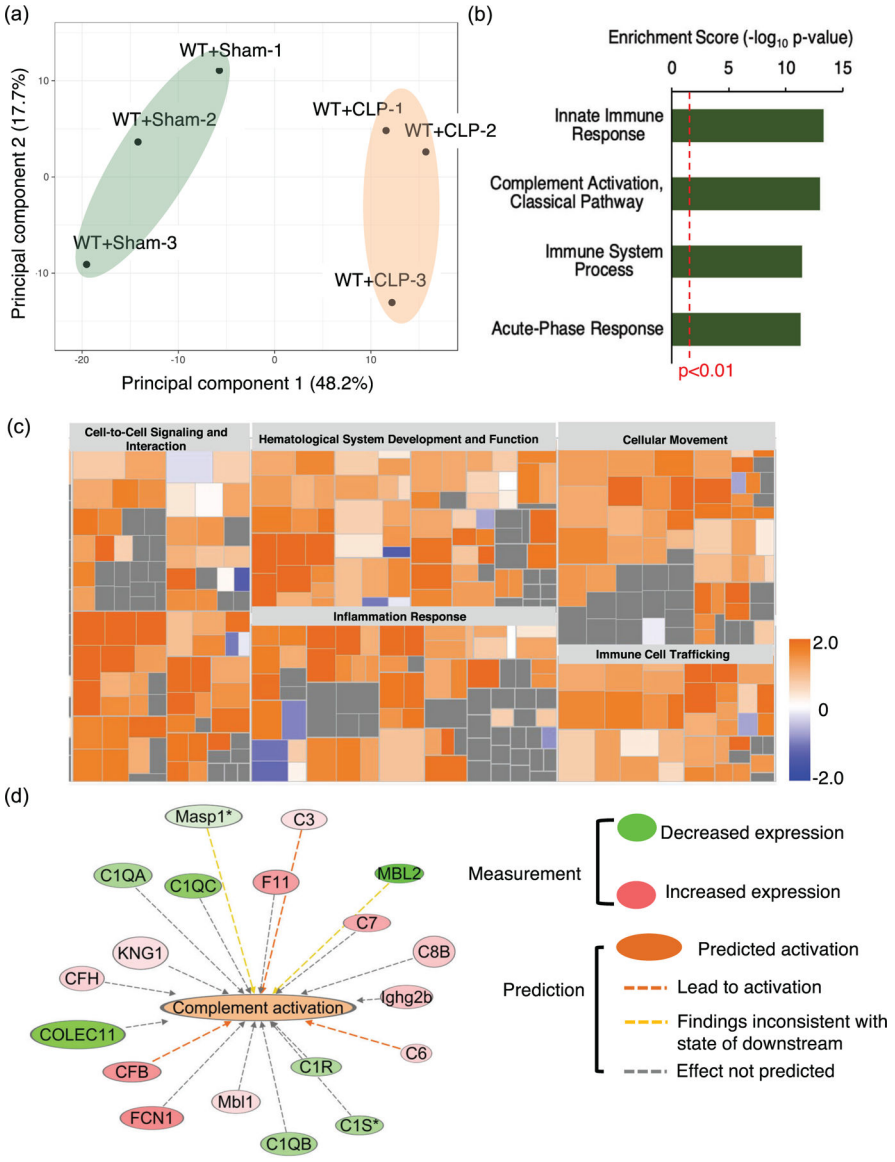

FIGURE 5.

Septic injury induces significant changes in EV palmitoyl-protein profile with complement pathway being the most activated pathway. (a) Principal component analysis shows that EVs collected from WT mice subjected to sham procedure cluster distinctly from EVs of WT mice subjected to CLP. $n = 3$ (b) GO biological process enrichment analysis of the EV palmitoylated proteins that are significantly changed by sepsis. The sepsis-altered palmitoylated proteins are highly enriched in immune responses. (c) IPA heatmap shows the predicted effects of sepsis-altered EV palmitoylated proteins on diseases/functions. Colour is defined by IPA *z*-score, with orange being predicted activation and blue being predicted inhibition. Size is defined by the −log(p-value) calculated by Fisher Exact Tests in IPA. (d) IPA prediction indicates the activation of complement pathway on EVs from CLP-treated mice compared to EVs from sham-treated mice. Septic injury-induced expression changes of

complement components are indicated by colour. Red: upregulated by septic injury, Green: downregulated by septic injury

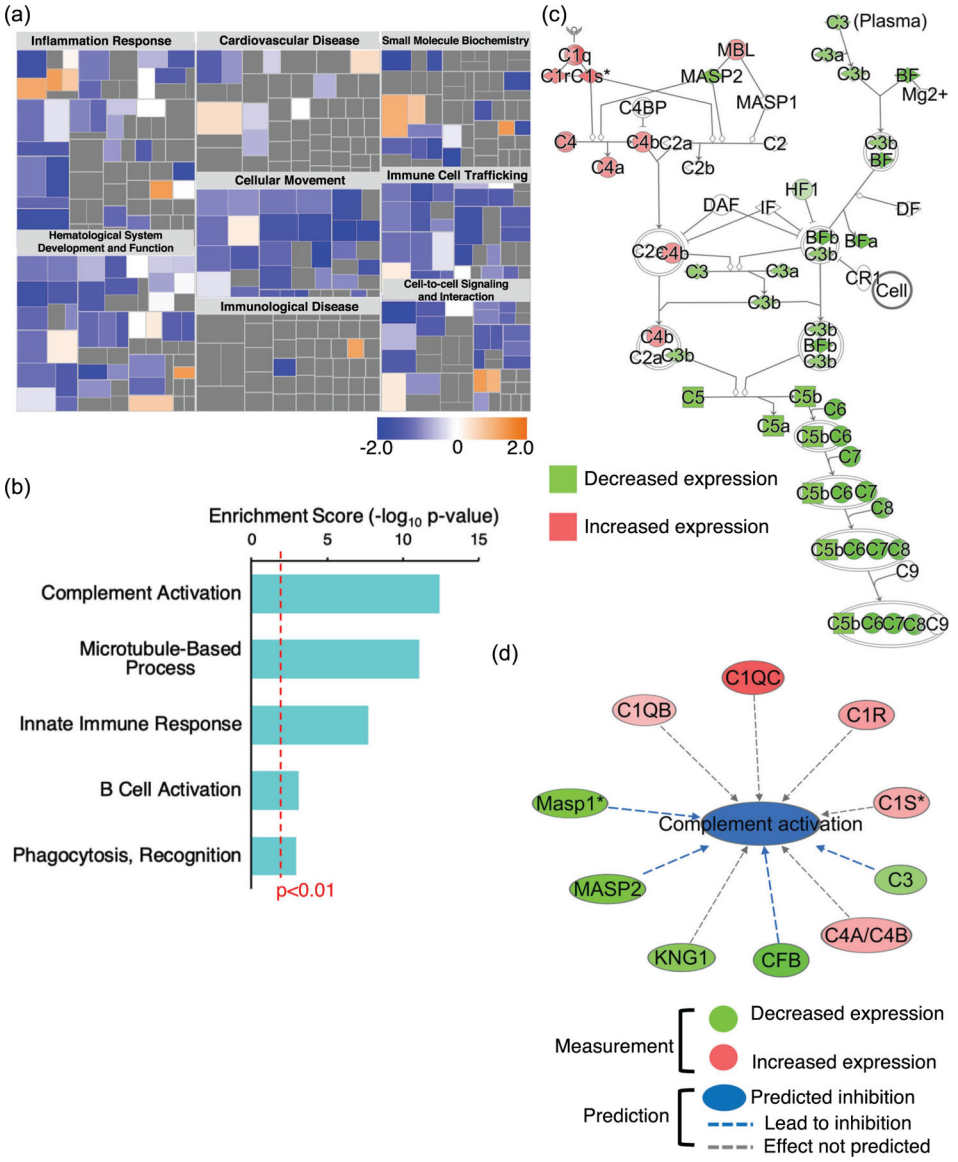

FIGURE 6. DHHC21 loss-of-function greatly attenuates septic injury-induced increase in complement components on EVs

. (a) IPA diseases and function analysis of DHHC21-altered EV palmitoylated proteins demonstrates DHHC21 functional deficiency exerts inhibitory effects on inflammatory pathways in EVs after septic injury. Colour is defined by IPA *z*-score, with orange being predicted activation and blue being predicted inhibition. Size is defined by the -log(*p*-value) calculated by Fisher Exact Tests in IPA. (b) GO biological process enrichment analysis of the EV palmitoylated proteins significantly changed by DHHC21 loss-of-function in septic injury. Complement activation shows the highest enrichment score. (c) IPA network displays the expression changes of complement components on EVs caused by DHHC21 functional deficiency after CLP. Expression change is measured by quantitative LC-MS/MS, $n = 3$. Green: downregulated by DHHC21 loss-of-function. Red: upregulated by DHHC21 loss-of-function. (d) IPA analysis of complement components significantly altered by DHHC21

after CLP. Prediction result indicates that DHHC21 loss-of-function attenuates septic injury-caused complement activation on EVs

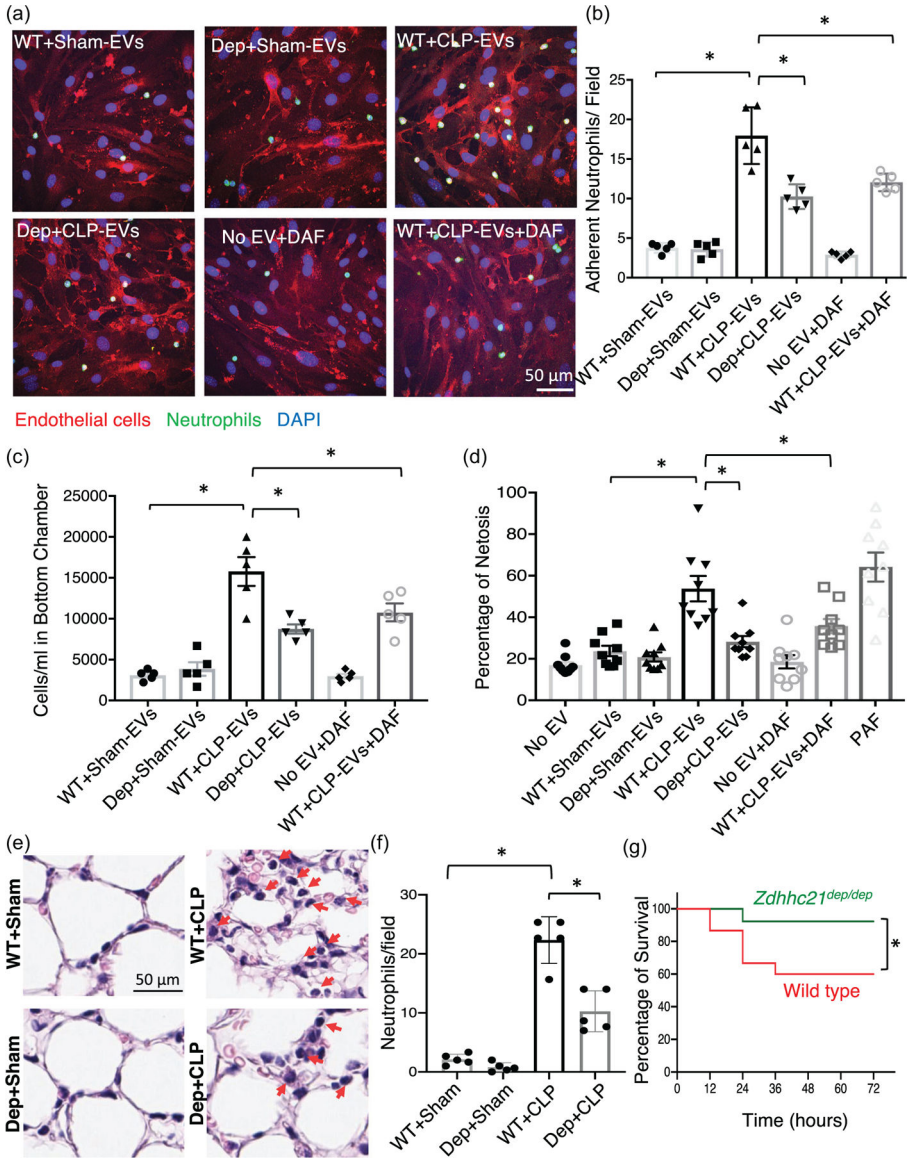

FIGURE 7.

EVs from *Zdhhc21*$^{dep/dep}$ mice after CLP exhibit impaired ability to induce neutrophil activation compared to EVs from WT mice after CLP. (a,b) EVs from WT mice with septic injury enhance neutrophil adhesion to TNF-α (100 ng)-pretreated endothelial cells, an effect attenuated by complement inhibitor DAF (10 μg/ml) and DHHC21 functional deficiency. (a) Representative images of leukocyte adhesion. (b) Quantification of adherent neutrophils per field. Results are presented as mean ± SEM. $n = 5$ independent experiments, and four fields of view are imaged and analyzed per experiment. (c) Complement inhibitor DAF and DHHC21 deficiency block neutrophil transendothelial migration caused by EVs from CLP-challenged WT mice. Results are presented as mean ± SEM, $n = 5$ (d) NETosis caused by WT EVs after CLP is attenuated by complement inhibitor DAF and DHHC21 loss-of-function. PAF (20 μM) serves as a positive control for NET formation. Results are presented as mean±SEM, $n = 9$. *$p < 0.05$. (e) Representative images of lung tissues obtained from

mice 24 h after CLP. Red arrows indicate infiltrated neutrophils. (f) Quantification of infiltrated neutrophils. Results represent mean ± SEM from five mice. (g) Survival rate in mice subjected to CLP challenge (n = 15 mice)